8

Finite element modeling for a morphometric and mechanical characterization of trabecular bone from high resolution magnetic resonance imaging

Angel Alberich-Bayarri[1], Luis Martí-Bonmatí[1],
M. Ángeles Pérez[2], Juan José Lerma[3] and David Moratal[4]
[1]*Department of Radiology, Hospital Quirón Valencia, Valencia, Spain.*
[2]*Group of Structural Mechanics and Materials Modeling, Instituto de Investigación en Ingeniería de Aragón, Universidad de Zaragoza, Zaragoza, Spain.*
[3]*Department of Rheumatology, Hospital Quirón Valencia, Valencia, Spain.*
[4]*Center for Biomaterials and Tissue Engineering, Universitat Politècnica de València, Valencia, Spain.*

1. Introduction

Trabecular bone disorders such as osteoporosis are currently becoming a worldwide concern, affecting nearly 200 million of people (Reginster & Burlet, 2006). This syndrome is characterized by a diminution of the bone density and also deterioration in the trabecular bone architecture, both factors inducing an increased bone fragility and higher risk to suffering skeletal fractures. The current diagnosis of osteoporosis disease is based on bone mineral density (BMD) measurements, which are obtained using Dual emission X-ray Absorptiometry (DXA) techniques and do not provide any information about the trabecular bone properties at structural level. Although it is accepted that low BMD increases fracture risk, not all patients who are osteoporotic will sustain a fracture. Low BMD as a risk factor for fracture can be compared to high cholesterol as a risk factor for heart disease, being BMD a rather poor predictor of fracture risk (Wehrli et al., 2007). In fact, a large analysis showed that, on the average, BMD explains about 60% of bone strength (Wherli et al., 2002).
The majority of bone fractures associated with osteoporosis take place in vertebrae, hip or wrist. In the European Union, in the year 2000, the number of osteoporotic fractures was estimated at 3.79 million, of which 24% were hip fractures (Kanis & Johnell, 2004). Of all fractures due to osteoporosis, hip fractures are the ones that are most disabling. In 1990, about 1.7 million new hip fractures occurred worldwide, and this figure is expected to rise to 2.6 million by 2025 (Gullberg et al., 1997). Furthermore, women who have sustained a hip fracture have a 10% to 20% higher mortality than would be expected for their age (Cummings & Melton, 2002).

Fractures are the consequence of mechanical overloading. The evaluation of elasticity and fluency limits of different materials and structures is commonly assessed by mathematics and engineering techniques. It seems reasonable to consider that bone fracture risk should also be analyzed by exact and precise engineering methods. Nevertheless, although bone mechanical properties can be directly extracted from *ex vivo* experiments, the mechanical analysis of bone *in vivo* has always been limited to indirect measurements since there is no physical interaction with the sample. These indirect measurements have evolved through time, being initially age and sex two good indicators of bone health. Nowadays, the most extended measure of bone quality is the BMD measured using DXA techniques. In fact, the DXA technique has been shown to be accurate, precise and reproducible in the BMD quantification. However, other imaging-based techniques that work at microstructural level are of high interest in the evaluation of bone microarchitecture quality. Therefore, the investigation in new methods to characterize trabecular bone microarchitecture alterations produced by the disease is crucial. Such advances may not only be useful for a better diagnosis of the disease, but also to evaluate the efficacy of the existing therapies.

The advances of digital radiology and modern medical imaging techniques like computed tomography (CT), high-resolution peripheral quantitative computed tomography (HR-pQCT) and magnetic resonance imaging (MRI) have allowed the research of *in vivo* characterization of bone microarchitecture (Ito et al., 2005; Boutroy et al., 2005). Although a high sensitivity to bone tissue structure is appreciated in X-Ray based techniques, like CT or HR-pQCT which can achieve very high spatial resolutions, the high inherent contrast between bone and bone marrow and its non-ionizing radiations places MRI as an appropriate technique for the *in vivo* characterization of cancellous bone.

Recent high field MRI scanners permit the acquisition of images with a high spatial resolution, in combination with satisfactory signal-to-noise ratio (SNR) and contrast-to-noise ratio (CNR). In fact, the higher spatial resolutions achievable with high field 3 Tesla MR scanners allow the development of reliable three-dimensional (3D) reconstructions of tissues with the possibility of applying engineering-based methodology to simulate structures and behaviours under certain conditions. The finite element (FE) method is the most extended mathematical tool for complex modelling and simulations and it has been widely applied to civil, spatial and many different engineering disciplines. This method can also be used in biomedical engineering for the simulation of organs and tissues under different scenarios (Prendergast, 1997). In the case of bone tissue, the combination of high quality image acquisitions with proper image post-processing and computational based mechanical simulations using FE with reduced element size, also called micro-FE (μFE), will improve osteoporosis characterization, reinforce the diagnosis process, and perform an accurate evaluation of the response to different therapies (Ito et al., 2005; Boutroy et al., 2005; Alberich-Bayarri et al., 2008).

In the present chapter, the process for trabecular bone mechanical simulation and analysis from high spatial resolution MRI acquisitions is detailed. Results of the FE application to healthy and osteoporotic populations are also shown.

2. Image acquisition and processing

Image acquisition

Due to the high spatial resolutions required for the assessment of trabecular bone tissue, SNR tends to be significantly reduced in MRI acquisitions. There exists a number of imaging problems inherent to the use of high spatial resolution MRI where technical parameters have to be considered. The best MRI configuration for proper acquisitions of the trabecular bone region is based on 3D gradient echo (GRE) pulse sequences with reduced echo-time (TE), repetition time (TR) and flip angle (α) in order to obtain a high contrast between bone and surrounding bone marrow. A high SNR is achieved with the shortest TE and the use of phased array surface coils that can cover the entire region under analysis. In terms of acquisition quality, an appropriate area for the trabecular bone examination is the wrist region, which can be easily surrounded by the receiving coil and the sample – receptor distance is minimized. Metaphyses of the ulna and radius in the wrist region are rich in trabecular bone tissue. Acquired images obtained at metaphyseal level of the radius have a high detail of the bone trabeculae, as it can be appreciated in figure 1.

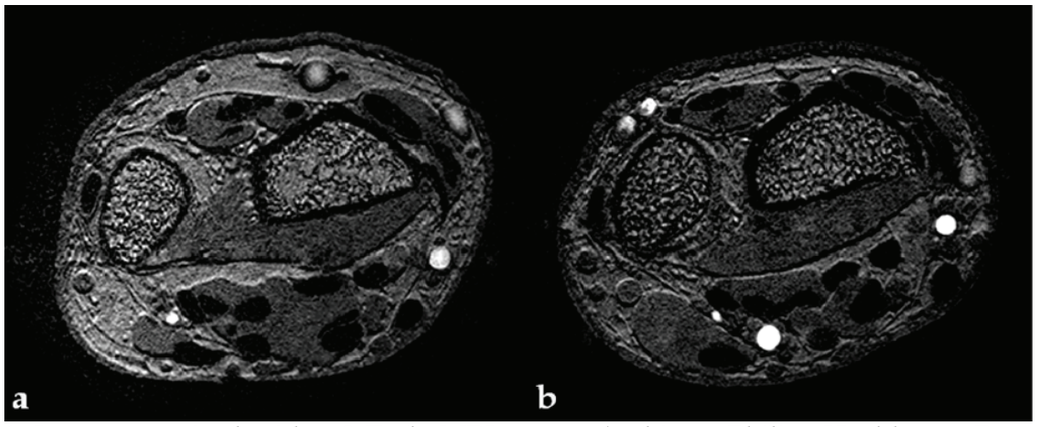

Fig. 1. Images acquired with a 3 Tesla MRI system (Achieva, Philips Healthcare, Best, The Netherlands). In a), wrist slice corresponding to the acquisition performed in a left-handed 62 years old female patient with osteoporosis. In b), image corresponding to a series acquired in a left-handed 64 years old female healthy volunteer.

In the examples shown in figure 1, acquired images have a very high spatial resolution, with an isotropic voxel size of 180 x 180 x 180 μm^3, which is even higher than the achievable with modern multi-detector CT scanners. However, the use of surface coils in the acquisitions produce slight modulations of the signal intensities across the images, also known as coil shading phenomena. Furthermore, although a high spatial resolution of 180μm was used, achieved voxel size was slightly larger than typical thickness of the trabeculae, which is about 100-150 μm. As it can be concluded, although the images have a very good quality, some pre-processing must be applied before 3D reconstruction, meshing and simulation of the trabecular bone structures.

Segmentation

Segmentation of the trabecular bone from MR images is performed by placing a rectangular region of interest (ROI) in the first slice corresponding to the most proximal position and

thereafter propagated to the rest of slices. Segmented areas must be verified to exclusively contain marrow and trabecular bone (Figure 2-a).

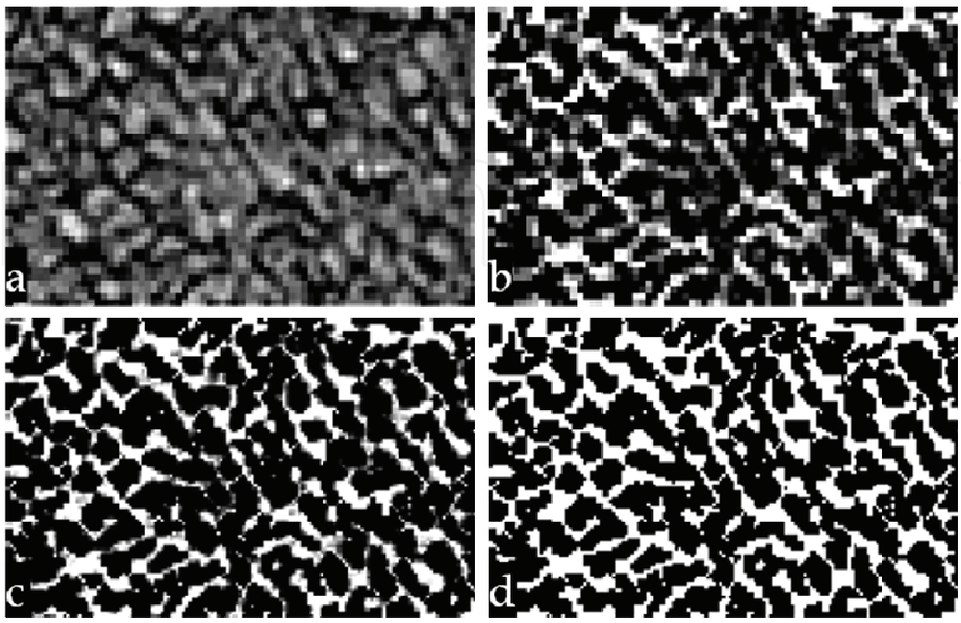

Fig. 2. Representative images resulting from the application of the different pre-processing algorithms. Example of the isolated region exclusively containing trabecular bone and marrow (a). Image resulting from the application of the coil shading correction through the local intensities determination (b). Interpolated image after the execution of the sub-voxel processing algorithm for an apparently increased spatial resolution (c). Binarized image obtained at the end of the pre-processing chain where only complete bone or marrow voxels exist (d).

Coil heterogeneities correction

Slight modulations of the signal intensities across the acquisition volume, also known as coil shading phenomena, are corrected with nearest-neighbour statistics by the application of an implemented 3D local thresholding algorithm (LTA), as a generalization from its 2D version (Vasilic & Wehrli, 2005). Marrow intensity values in the neighbourhood of each voxel are determined and bone voxels intensities are scaled using calculated local intensities. Concretely, the method is based on the calculation of the average Laplacian values $\langle \tilde{L} \rangle_{\vec{r}}(I)$ in a sphere region $S(\vec{r})$ with a radius R=15 pixels, being I the voxel intensity and $\vec{r}$ the center of the sphere, which is displaced through all voxels of the volume. When the calculated Laplacian equals zero $\langle \tilde{L} \rangle_{\vec{r}}(I_t(\vec{r})) = 0$, the corresponding marrow intensity $I_t(\vec{r})$ can be determined locally. After the marrow intensity is obtained, it is used as a threshold and voxels can be directly classified into pure marrow voxels or scaled by its local threshold value and labeled as partially occupied by bone voxels (Figure 2-b).

Sub-voxel processing

The extreme conditions in terms of low SNR and partial volume effects due to larger voxel size than typical thickness of the trabeculae, which is about 100-150μm, forced the

implementation of a method to increase the reconstructed spatial resolution. A subvoxel-processing algorithm is applied to minimize partial volume effects and therefore improving the cancellous bone structural quantification from MR images (Hwang & Wehrli, 2002). The method consists on a two-pass algorithm where each voxel is initially divided into eight subvoxels which are assigned a level of intensity conditioned by the corresponding level of their voxel and near subvoxels, and also under the assumption that the amount of bone intensities must be conserved. In the first pass of the algorithm, each subvoxel is assigned an intensity value depending on the intensities of the adjacent voxels and the local sum of intensities. The second pass of the algorithm consists on the refinement of the previously calculated subvoxel intensities considering the intensities of the neighbouring subvoxels and the total amount of intensity conservation. Finally, an increased apparent isotropic spatial resolution of 90 μm is achieved and partial volume effects are minimized (Figure 2-c).

Binarization
Resulting images are binarized into exclusively bone or marrow voxels (Figure 2-d). Histogram shape-based thresholding is applied through the Otsu's method implemented in 3D. The method consists in the minimization of the intra-class variance of volume intensities (Otsu N., 1979), which has been shown to be equivalent to maximizing the between-class variance. Thus, the optimum separation threshold is calculated for the entire volume using:

$$t^* = \arg.\max_t \frac{\sigma^2{}_B}{\sigma^2{}_T} \tag{1}$$

where $\sigma^2{}_T$ is the total variance and $\sigma^2{}_B$ is the between-class variance. The optimum binarization threshold is t^*. Finally, voxels can be classified as bone or marrow depending on their intensity value.

3. Volumetric reconstruction and meshing

Once the region under analysis has been binarized, a logical 3D matrix is obtained, with bone voxels represented by 1's and marrow voxels by 0's. For visualization, the volume is smoothed by a three-dimensional routine and the marching cubes algorithm (Lorensen & Cline, 1987) is then applied in order to obtain a volumetric reconstruction of the structure, as can be seen in figure 3.
Depending on the model to be simulated, different element types can be used to construct the mesh. Two-dimensional (2D) surface based meshes are usually compound of triangles or quadrilaterals. Considering a trabecular bone structure, a 3D volume mesh needs to be generated for a volumetric simulation and evaluation of trabeculae mechanical resistance. Volume meshes are usually compound of solid elements such as tetrahedrons and hexahedrons. Isotropic hexahedrons with 8 nodes are usually referred as brick elements.
To develop an efficient meshing of the trabecular bone structure, brick elements are the best option in terms of computational burden. The 3D reconstruction is conserved and a more efficient stress analysis can be implemented (Alberich-Bayarri et al., 2007).

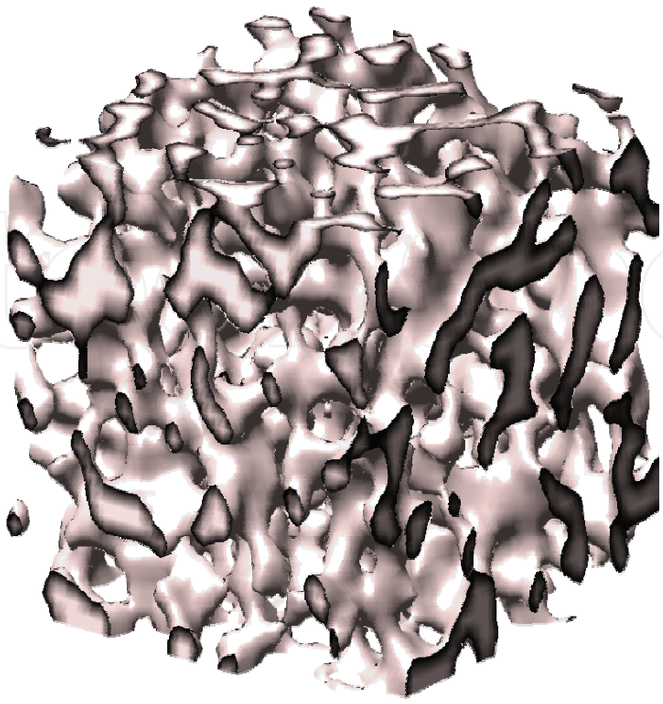

Fig. 3. Smoothed 3D reconstruction of the trabecular bone obtained from the application of volume rendering algorithms to the binary volume of data.

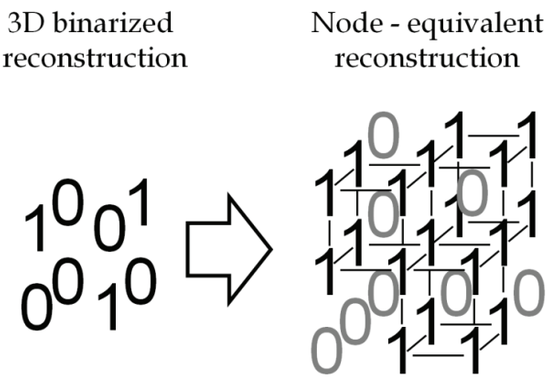

Fig. 4. Example showing the algorithm basis for conversion from the 3D binarized matrix into a 3D matrix containing the node information of the structure. Node coordinates and element connectivity extraction from this process is straightforward.

An algorithm is needed to convert 3D reconstruction geometry information into FE structural data where node coordinates and element interconnections are detailed. Although a very intuitive algorithm would consist in the voxel-by-voxel sequential analysis of structural coordinates and corresponding connectivity, an optimized algorithm implemented by the authors is used for the mesh generation process.

The idea of this algorithm is a direct detection of nodes of the structure working completely with matrices and without sequentiality. Considering the 3D binarized reconstruction matrix of size m x n x p, a new matrix nodal equivalent matrix of size (m+1) x (n+1) x (p+1) is created and filled with zeros. Then, for each bone voxel found in the 3D binarized reconstruction, eight ones representing the nodes of the element are situated on the corresponding position of the node equivalent reconstruction (see Fig. 4). The extraction of the node coordinates from the node equivalent matrix is direct. The relationship between the original bone voxel and the corresponding calculated nodes is also conserved. The implemented meshing algorithm can build a mesh with 1048706 nodes and 285148 elements in 9.78 seconds using an Intel® Core™ 2 Quad CPU at 2.83 GHz and 8 Gb of RAM memory. At the end of the process, the lists containing the nodes with the corresponding coordinates and the elements with the corresponding node connectivity are completed and the FE mesh is fully defined.
Once the mesh is strictly defined, it must be assembled in a file to ease the importation from specific FE commercial software where the simulation is performed. Different FE tools like ANSYS (Ansys Inc., Southpointe, PA, USA) or ABAQUS (Simulia, Providence, RI, USA) are used for the FE model definition and posterior simulation.

4. FE model definition

The generated mesh must be prepared for the simulation after it has been imported in the FE software, that is, a model must be fully generated considering the bulk material properties, boundary conditions and loads application.
Initially, the bulk material properties for each element must be defined. In this case, elements composition is supposed to be formed by compact bone, with linear, elastic and isotropic behaviour. Numerically, the elastic properties of the material forming the elements consist of a Young's modulus given by E_b=10GPa and a Poisson's ratio of v=0.3 (Fung, 1993; Newitt et al., 2002).
Experimentally, resistance and elasticity properties of materials and other structures are evaluated by a compression essay using specific equipment in laboratory. Stress–strain relationship is analyzed and Young's modulus of the whole structure can be easily calculated from the linear slope of the stress–strain curve. Analogously, in the FE simulation, null displacement is imposed on nodes from one side while a total strain (ε) of 10% of the edge length is specified on nodes from the opposite side for the compression simulation. An iconography of the scenario to be modelled can be appreciated in figure 5.
The modelling of a trabecular bone uniaxial compression essay requires deciding the loading direction. In our case, in the radius bone, the principal orientation of the trabecular bone corresponds to the longitudinal dimension (Gullberg et al., 1997). Since an axial acquisition is performed for the images generation, the longitudinal direction corresponds to the MR scanner slice z direction. In this sense, a crucial advantage of 3 Tesla systems comparing with 1.5 Tesla is the capability of performing high resolution acquisitions not only in plane but also in slice direction (isotropic voxel size). In figure 6, a FE mesh of a trabecular bone structure loaded to the commercial package ANSYS 10.0 is shown. The boundary conditions and the strain application can be also appreciated in the figure.

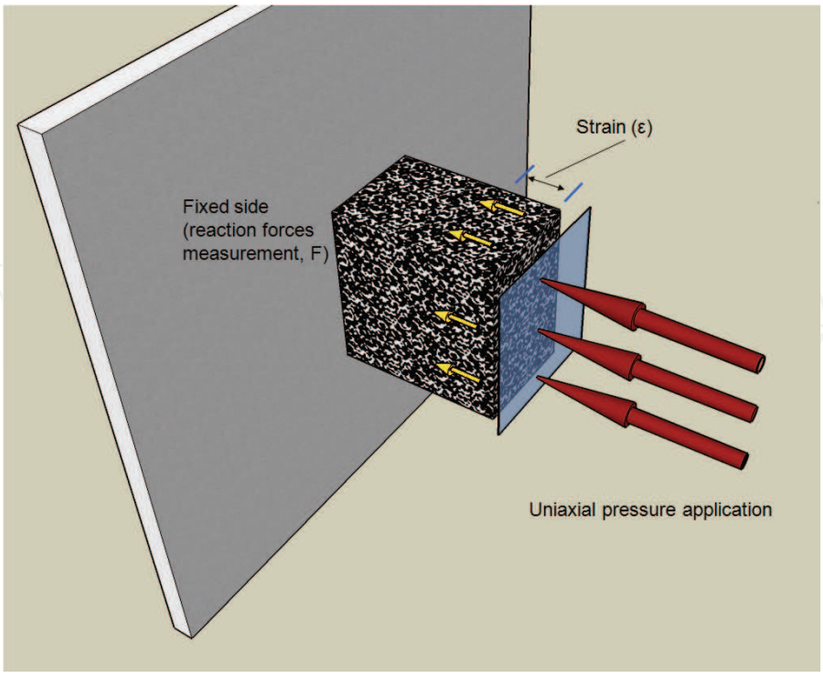

Fig. 5. Representation of the simulation applied using the FE method. A compression test is applied to the trabecular bone sample with a side fixed to a null displacement and the opposite side suffering an imposed deformation.

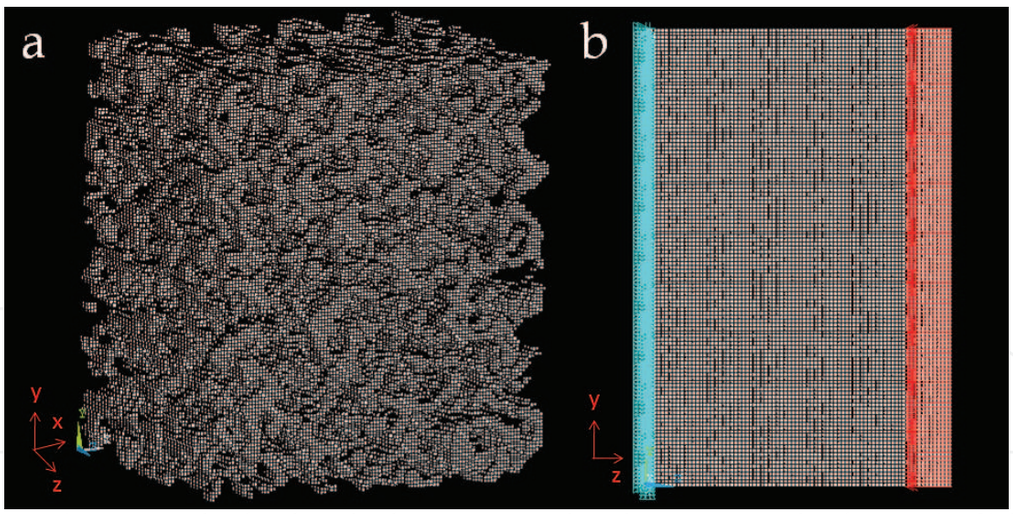

Fig. 6. In a), a FE mesh of trabecular bone imported in the commercial software ANSYS 10.0 is shown. The coordinates system is also shown, with the z direction corresponding to the longitudinal direction of the bone. In b), lateral view of the cancellous bone structure with boundary conditions definition, that is, null displacement on the left side (blue) and 10% strain in the right side (red).

Once the model is completely defined, including forces application, material properties and boundary conditions, simulation process is ready to begin.

5. Simulation and results calculation

The calculation of the mechanical results from the simulation is a very demanding task in terms of computational cost. The number of equations of our system is considerably high, since there are 3 degrees of freedom per node, and each element has 8 nodes. As an example, a mesh with 800000 nodes defines a system of 2400000 equations.
In order to solve the large systems of equations, different strategies can be used, depending on the kind of solver (sparse, conjugate gradients, minimal residual). In the present case, for the characterization of the trabecular bone response, systems are solved using a standard sparse solver.
Although the different techniques for handling the matrices and approaching to the final solution, the mathematical problem to be solved is summarized as follows (Zienkiewicz et al., 2006):

The stiffness matrix of each element K^e can be calculated by equation (2),

$$K^e = \int_{V^e} B^T D B \cdot d(vol) \tag{2}$$

where D is the elasticity matrix, which exclusively depends on Young's modulus and Poisson's ratio (see equation (3)) and B is a matrix containing spatial information.

$$D = \frac{E}{1-v^2}\begin{bmatrix} 1 & v & 0 \\ v & 1 & 0 \\ 0 & 0 & (1-v)/2 \end{bmatrix} \tag{3}$$

The global stiffness matrix of the structure under analysis can be assembled by equation (4), taking into consideration the stiffness matrix of each element.

$$K_{ij} = \sum K_{ij}^e \tag{4}$$

Once the stiffness matrix is assembled, the objective of the FE problem is to solve the structural equation (5), which relates the global stiffness matrix with the nodal displacements (u) and forces (f):

$$K \cdot u = f \tag{5}$$

After nodal displacements and forces are calculated, the calculation of stresses and strains is straightforward.

A very interesting parameter that can be extracted from the FE results is the apparent Young's modulus of the whole structure by the application of the homogenization theory (Hollister et al., 1991; Hollister & Kikuchi, 1992) and equation (6).

$$E_{app} = \frac{1}{\varepsilon A} \sum_{n} F \tag{6}$$

Where F corresponds to the nodal reaction forces measured in the fixed side, A is the area of the fixed side, and ε is the imposed strain.
Apparent Young's modulus (Eapp) is used as an estimation of cancellous bone resistance to compression.

6. Validation with sheep models

The mechanical trabecular bone biomarker parameters extracted from high resolution 3T MR images can be validated by a comparison with 64-MDCT and micro-CT derived parameters in the cancellous bone of sheep tibiae.
Five fresh legs were extracted from adult sheep cadavers in order to perform the trabecular bone analysis of the tibia. The samples were prepared after skin removal and cleaning for the MR and 64-MDCT acquisitions. The μCT examinations required the preparation of small trabecular bone samples that were extracted from the metaphysis of the sheep tibiae. Results of the Von Mises stress maps can be appreciated in an example in figure 7.

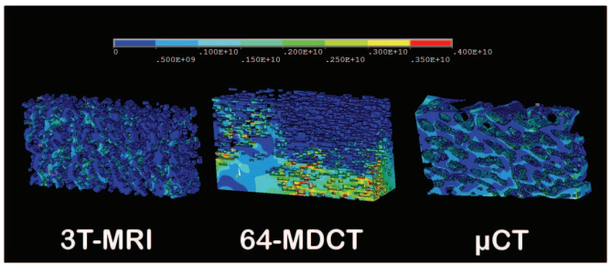

Fig. 7. Parametric reconstructions of the Von Mises nodal stress results for the compression simulation using three different modalities (3T-MRI, MDCT and μCT).

The values obtained for the analyzed parameters in the 3 acquisition modalities can be appreciated in Table 1. Setting micro-CT results as the reference, MR calculated elastic modulus were slightly smaller while CT derived elastic modulus were clearly much higher. This bone overestimation in MDCT acquisitions is probably due to the bone hyper estimation effect of the point spread function (PSF) at high spatial resolutions.

	Ex (MPa)	Ey (MPa)	Ez (MPa)
3T-MRI	79.910	320.160	827.390
MicroCT	105.920	485.911	995.390
MDCT-64	1122.509	1430.551	2577.300

Table 1. Results for the apparent Young's modulus obtained in a trabecular bone sample from the sheep legs.
The results obtained for the elastic modulus after compression FE test of the MR-derived mesh are more proximal to the calculated for micro-CT than the obtained from 64-MDCT. Compared to micro-CT, a bone overestimation is observed in the 64-MDCT calculated parameters, as previously mentioned. Similar stress distributions can be appreciated in

Figure 1 between 3T-MR and micro-CT while 64-MDCT derived stress map shows a high and non-uniform stress arrangement.

7. Application to healthy subjects and patients with osteoporosis

The Young's modulus parameter was initially evaluated in a healthy population in order to define a rank of normality for the parameter and evaluate differences between sex or age.
The Young's modulus results on a healthy population of 40 subjects showed significant differences between males and females ($p=0.012$) with lower values in females (143.02 ± 24.83 MPa vs. 241.58 ± 28.07 MPa, mean ± standard error of the mean (SEM), female and male respectively). Age showed no relationship with the Young's modulus parameter ($r^2=0.033$) (Alberich-Bayarri et al., 2008).
An interesting point is that the volume of analyzed bone had an influence on the elasticity results. There was a statistically significant difference ($p<0.001$, ANOVA test) between Eapp results obtained for the large volume of interest (VOI) and those obtained for a small VOI (189.84 ± 20.02 vs. 81.56 ± 16.86, mean ± standard deviation). Furthermore, as it can be appreciated in figure 8, differences between Eapp results for the two different volumes analyzed become greater when the values of the elastic parameter grow. The reason for small VOI analysis was the minimization of the computational burden in compression simulation. However, it was shown that the goodness of the results diminished as the restricted volume dimensions decreased (Alberich-Bayarri et al., 2008). Authors detected that the mechanical analysis results applied to the large sample volumes of trabecular bone better characterized its properties, with significant differences between male and female subjects for Young's modulus. As expected, Eapp results were greater in men (Keaveny & Yeh, 2002).

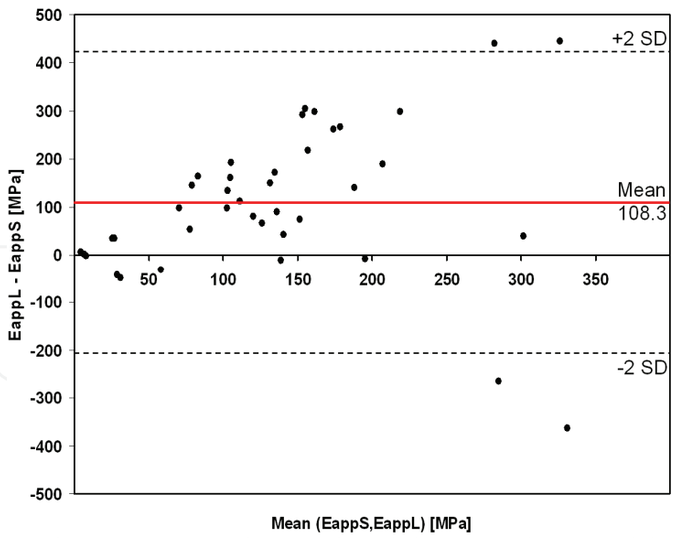

Fig. 8. Bland-Altman plot comparing the results of the Eapp for two different VOI analyzed, the large volume (L) and the small volume (S). (adapted from Alberich-Bayarri et al.).

Authors' results for the mean elastic modulus were lower than the value obtained for the uniaxial compression (Newitt D.C. et al., 2002) (189.84 ± 126.62 MPa vs. 2050 ± 590 MPa, respectively). However, these differences are probably due to different acquisition

configurations. In this sense, author's results are close to those obtained by (Dagan et al., 2002) with an Eapp of 150 MPa. In conclusion, acquisition technique and processing tools clearly influence the Eapp values.
Also, the same methodology was applied to a population of 20 female osteoporosis patients in order to evaluate Young's modulus sensitivity to the disease. Mean Young's modulus computed for the osteoporotic population and a paired reference subjects is shown in table 2.

Parameter	Healthy (n=21)	Patients (n=20)
Eapp (MPa)	142 ± 25	43.1 ± 24.8

Table 2. Young's modulus results in a population of healthy volunteers and a group of patients with Osteoporosis.

Resultant Von Mises stress parametric maps were also qualitatively different between healthy and osteoporotic subjects. While healthy volunteers present a uniform structural response to compression, with a distributed stresses, in the case of patients with osteoporosis the parametric reconstructions showed a high heterogeneity with a specific zone of high stress and resulting in a less resistant structure.

8. Conclusions and future challenges

Although further evaluation is needed about the usefulness of these methods in osteoporosis, it seems clear that computational generated 3D models of the cancellous bone from high resolution 3 Tesla MRI can be used to characterize bone *in vivo*, analyzing different mechanical conditions of the cancellous microstructure.
The FE analysis could be performed in a more complex philosophy, if bone anisotropy is considered for bulk material properties definition (Hellmich et al., 2008), and also if not only the part with linear behaviour of the stress–strain curve is considered, but also the curve region showing plasticity or non-recoverable deformation. These studies should add more information to the mechanisms involved in bone fracture, like buckling phenomena, just before the breaking point arrives.
Patients are classified nowadays using the World Health Organization (WHO) criteria, depending on the amount of bone loss, in osteopenic or osteoporotic patient. These are the clinical references used for new biomarkers evaluation. However, multivariate studies may provide different groups or classification patterns for the patient populations.
Results of the mechanical simulations among a large population should provide knowledge for the establishment of new biomarkers of disease. New clinical trials and studies should help to analyze the sensitivity of these parameters to the treatment.

Acknowledgements

The support of the Spanish Ministry of Science and Innovation through project TEC2009-14128 and of the Generalitat Valenciana through projects GV/2009/126 (grups d'investigació emergents) and ACOMP/2010/022 (ajudes complementàries) is acknowledged. The funding from Instituto de la Mediana y Pequeña Industria Valenciana (IMPIVA) of the Generalitat Valenciana (IMIDTP/2009/334) is also acknowledged.

9. References

Alberich-Bayarri, A.; Moratal, D.; Martí-Bonmatí, L.; Salmerón-Sánchez, M.; Vallés-Lluch, A.; Nieto-Charques, L. & Rieta JJ. (2007). Volume mesh generation and finite element analysis of trabecular bone magnetic resonance images. *Proceedings of: Annual International Conference of the IEEE Engineering in Medicine and Biology Society,* pp. 1603-1606, 1557-170X, Lyon, France, August 2007, *IEEE Engineering in Medicine and Biology Society*.

Alberich-Bayarri, A.; Marti-Bonmati, L.; Sanz-Requena, R.; Belloch, E. & Moratal, D. (2008). In vivo trabecular bone morphologic and mechanical relationship using high-resolution 3-T MRI. *American Journal of Roentgenology,* 191, 3, (Sep 2008) 721-726, 0361-803X.

Boutroy, S.; Bouxsein, M.L.; Munoz, F. & Delmas, P.D. (2005). In vivo assessment of trabecular bone microarchitecture by high-resolution peripheral quantitative computed tomography. *The Journal of clinical endocrinology and metabolism*, 90, 12 (Dec 2005), 6508–6515, 0021-972X.

Cummings, S.R. & Melton III, J.R. (2002). Epidemiology and outcomes of osteoporotic fractures. *Lancet,* 359, 9319 (May 2002), 1761–1767, 0140-6736.

Fung, Y.C. (1993). Biomechanics. *Mechanical properties of living tissues*, pp. 500-518, 2nd ed, Springer, New York, NY.

Dagan, D.; Be'ery, M. & Gefen, A. (2004). Single-trabecula building block for large-scale finite element models of cancellous bone. *Medical & biological engineering & computing*, 42, 4 (Jul 2004), 549-556, 0140-0118.

Geraets, W.G.; Van der Stelt, P.F.; Lips P.; Elders P.J.; Van Ginkel F.C. & Burger E.H. (1997). Orientation of the trabecular pattern of the distal radius around the menopause. *Journal of Biomechanics*. 30, 4 (Apr 1997), 363-370, 0021-9290.

Gullberg, B.; Johnell, O. & Kanis, J.A. (1997). World-wide projections for hip fracture. *Osteoporosis International*, 7, 5, 407–413, 0937-941X.

Hellmich, C.; Kober, C. & Erdmann, B. (2008). Micromechanics-based conversion of CT data into anisotropic elasticity tensors, applied to FE simulations of a mandible. *Annals of biomedical engineering*, 36, 1 (Jan 2008), 108–122, 0090-6964.

Hollister, S.J.; Fyhrie, D.P.; Jepsen, K.J. & Goldstein, S.A. (1991). Application of homogenization theory to the study of trabecular bone mechanics. *Journal of biomechanics*, 24, 9, 825–839, 0021-9290.

Hollister, S.J. & Kikuchi, N. (1992). A comparison of homogenization theory and standard mechanics analyses for periodic porous composites. *Computational Mechanics,* 10, 2 (Mar 1992), 73–95, 0178-7675.

Hwang, S.N. & Wehrli, F.W. (2002). Subvoxel processing: a method for reducing partial volume blurring with application to in vivo MR images of trabecular bone. *Magnetic Resonance in Medicine*, 47, 5 (May 2002), 948-957, 0740-3194.

Ito, M.; Ikeda, K.; Nishiguchi, M.; Shindo, H.; Uetani, M.; Hosoi, T. & Orimo, H. (2005). Multi-detector row CT imaging of vertebral microstructure for evaluation of fracture risk. *Journal of bone and mineral research : the official journal of the American Society for Bone and Mineral Research,* 20, 10 (Oct 2005), 1828-1836, 0884-0431.

Kanis, J.A. & Johnell, O. (2005). Requirements for DXA for the management of osteoporosis in Europe. *Osteoporosis International,*16, 3 (Mar 2005), 229–238, 0937-941X.

Keaveny, T.M. & Yeh, O.C. (2002). Architecture and trabecular bone - toward an improved understanding of the biomechanical effects of age, sex and osteoporosis. *Journal of musculoskeletal & neuronal interactions*, 2, 3 (Mar 2002), 205-208, 1108-7161.

Lorensen, W.E. & Cline, H.E. (1987). Marching Cubes: A high resolution 3D surface construction algorithm. *Computers & Graphics*, 21, 4 (July 1987), 163-169, 0097-8493.

National Institutes of Health. (2000). Osteoporosis Prevention, Diagnosis, and Therapy. *Consensus Development Conference Statement*. 17, 1 (March 27-29, 2000), 1-45.

Newitt, D.C.; Majumdar, S.; van Rietbergen, B.; von Ingersleben, G.; Harris, S.T.; Genant, H.K.; Chesnut, C.; Garnero, P. & MacDonald, B. (2002). In vivo assessment of architecture and micro-finite element analysis derived indices of mechanical properties of trabecular bone in the radius. *Osteoporosis International*, 13, 1 (Jan 2002), 6-17, 0937-941X.

Otsu, N. (1979). A threshold selection method from gray-level histogram. *IEEE Transactions on Systems, Man, and Cybernetics*, 9, 1, 82-86, 1083-4427.

Prendergast, P.J. (1997). Finite element models in tissue mechanics and orthopaedic implant design. *Clinical biomechanics (Bristol, Avon)*, 12, 6 (Sep 1997), 343-366, 0268-0033.

Reginster, J.Y. & Burlet, N. (2006). Osteoporosis: a still increasing prevalence. *Bone,* 38, 2 Suppl 1 (Feb 2006), S4-9, 8756-3282.

Vasilic, B. & Wehrli, F.W. (2005). A novel local thresholding algorithm for trabecular bone volume fraction mapping in the limited spatial resolution regime of in-vivo MRI. *IEEE transactions on medical imaging,* 24, 12 (Dec 2005), 1574-1585, 0278-0062.

Wehrli, F.W.; Saha, P.; Gomberg, B.; Song, H.K.; Snyder, P.J.; Benito, M.; Wright, A. & Weening, R. (2002). Role of magnetic resonance for assessing structure and function of trabecular bone. *Topics in magnetic resonance imaging : TMRI,* 13, 5 (Oct 2002), 335–355, 0899-3459.

Wehrli, F.W. (2007). Structural and functional assessment of trabecular and cortical bone by micro magnetic resonance imaging. *Journal of magnetic resonance imaging : JMRI*, 25, 2 (Feb 2007), 390-409, 1053-1807.

Zienkiewicz, O.C.; Taylor, R.L. & Zhu, J.Z. (2006). *The finite element method, its basis & fundamentals.* 6th edition. Elsevier, Oxford, UK. 2006. 0750663200.

Finite Element Analysis

Edited by David Moratal

ISBN 978-953-307-123-7

Hard cover, 688 pages

Publisher Sciyo

Published online 17, August, 2010

Published in print edition August, 2010

Finite element analysis is an engineering method for the numerical analysis of complex structures. This book provides a bird's eye view on this very broad matter through 27 original and innovative research studies exhibiting various investigation directions. Through its chapters the reader will have access to works related to Biomedical Engineering, Materials Engineering, Process Analysis and Civil Engineering. The text is addressed not only to researchers, but also to professional engineers, engineering lecturers and students seeking to gain a better understanding of where Finite Element Analysis stands today.

InTech Europe
University Campus STeP Ri
Slavka Krautzeka 83/A
51000 Rijeka, Croatia
Phone: +385 (51) 770 447
Fax: +385 (51) 686 166
www.intechopen.com

InTech China
Unit 405, Office Block, Hotel Equatorial Shanghai
No.65, Yan An Road (West), Shanghai, 200040, China
中国上海市延安西路65号上海国际贵都大饭店办公楼405单元
Phone: +86-21-62489820
Fax: +86-21-62489821

IntechOpen